Two-step spin crossover in Hofmann-type coordination polymers [Fe(2-phenylpyrazine)$_2${M(CN)$_2$}$_2$] (M = Ag, Au)

*Volodymyr M. Hiiuk,[†€] Sergii I. Shylin,[‡] Diana D. Barakhtii,[†] Dmytro M. Korytko,[†] Volodymyr O. Kotsyubynsky,[§] Aurelian Rotaru,[ǀ] Sergiu Shova,[#Δ] and Il'ya A. Gural'skiy[†]**

[†]Department of Chemistry, Taras Shevchenko National University of Kyiv, 64 Volodymyrska St., 01601 Kyiv, Ukraine.

[€]Faculty of Natural Sciences, National University of Kyiv-Mohyla Academy, 2 Skovorody St., 04070 Kyiv, Ukraine.

[‡]Department of Chemistry – Ångström Laboratory, Uppsala University, 75120 Uppsala, Sweden.

[§]Department of Material Science and New Technology, Vasyl Stefanyk Precarpathian National University, 57 Shevchenko St., 76018 Ivano-Frankivsk, Ukraine.

[ǀ]Faculty of Electrical Engineering and Computer Science & Research Center MANSiD, Stefan cel Mare University, 13 Universitatii St., 720229 Suceava, Romania.

[#]Ningbo University of Technology, No. 201, Fenghua Road, Ningbo City, Zhejiang, 315211, China.

[Δ]"Petru Poni" Institute of Macromolecular Chemistry, 41A Aleea Gr. Ghica Voda, 700487 Iasi, Romania.

ABSTRACT: Two 2D Hofmann-type complexes of composition [Fe(*Phpz*)$_2${M(CN)$_2$}$_2$] (where *Phpz* = 2-phenylpyrazine; M = Ag, Au) have been synthesized and their spin-crossover (SCO) behavior has been thoroughly characterized. Single crystal X-ray analysis reveals that these complexes contain a crystallographically unique Fe(II) center surrounded by two axial 2-phenylpyrazine ligands and four equatorial cyanide [M(CN)$_2$]$^-$ bridges. It is shown that using of a ligand with two aromatic rings, an advanced system of weak supramolecular interactions (metal-metal, C–H···M and π···π stacking contacts) is realized. This ensures additional stabilization of the structures and the absence of a solvent accessible voids due to dense packing. Both complexes are characterized by highly reproducible two-step SCO behavior, as revealed by different techniques (SQUID magnetometry, optical microscopy, etc.). Research shows the exceptional role of the presence of various supramolecular interactions in the structure and the influence of the bulky substituent in the ligand on SCO behavior. Moreover, the perspective of substituted pyrazines for the design of new switchable materials is supported by this work.

■ INTRODUCTION

Coordination compounds of the mid-first-row transition metals with nitrogen-containing ligands keep their relevance among researchers for many years because of the versatility of their magnetic behavior. This includes unique ability of these systems to reversibly switch between high-spin (HS) and low-spin (LS) electronic states of the central metal ion under the influence of external factors (temperature, pressure, guest molecule insertion, etc.). This phenomenon is usually referred as spin crossover (SCO).[1–5] The variety of properties affected by the spin transition defines a wide

range of proposed practical applications for these materials: thermochromic elements, nano-sized chemical memory units, chemical sensors, microwave switches, microelectronic devices, magnetooptical materials etc..[6–16] Multi-step SCO (with two or more steps) are interesting for understanding the nature of short-range interactions (steric and electronic), and longer-range packing effects on the cooperativity. In addition, understanding the nature of multi-step SCO may help in developing more advanced functional materials. The multi-step SCO can be caused by two different structural reasons: the presence of non-equivalent metal centers which undergo SCO at different temperatures[17–21] and the symmetry breaking within the structure caused by a change in the space group or various host-host/host-guest interactions which stabilize intermediate states between purely HS and LS states.[22–29] It is worth mentioning a number of cases when the nature of the two-step SCO remains enigmatic since the complexes contain one crystallographically unique Fe(II) center at all temperatures, and the values of all structural parameters (including bond lengths and angles) have an "average" HS/LS character at the plateau.[30–32]

To date, quite a few examples of materials showing multi-step SCO behavior are known.[17–27,30–46] There are several examples of three-,[37–39] four-,[23,25,26,40–45] six/five-[27] and even an example of a seven/eight-step[46] spin transition. It should be noted that significant number of such systems are Hofmann clathrate analogues, especially with dicyanometallic $[M(CN)_2]^-$ (M = Ag, Au) fragments and pyridine derivatives (ranging from simple monosubstituted to more complicated ligand systems).[2,8] In these complexes Fe(II) ions have a pseudo-octahedral coordination environment $[FeN_6]$ with two axial azine ligands and four dicyanometallic $[M(CN)_2]^-$ fragments that occupy equatorial positions. Significant advances in the production of multi-step 3D SCO systems have been achieved by Tong et al.[23,25,26,32,46,47] They showed that the use of various long bent pillaring ligand systems, as well as the introduction of different guest molecules, leads to distortions in

coordination framework (including due to various interactions host-guest), which leads to the symmetry breaking required for a multi-step SCO.

Some Hofmann clathrate analogues based on fused bicyclic azine ligands also display multi-step SCO behavior. For example, the use of isoquinoline ligand (*isoq*) makes it possible to obtain a complex of composition [Fe(*isoq*)$_2${Au(CN)$_2$}$_2$], which exhibits tristability for its spin states in a wide temperature range and contains three inequivalent Fe(II) sites.[34] Using 2,6-naphthyridine (*2,6-naphthy*), it is possible to obtain both a complex with a relatively abrupt two-step SCO in the temperature range 150–215 K, [Fe(*2,6-naphthy*){Ag(CN)$_2$}{Ag$_2$(CN)$_3$}], and a complex with an incomplete one-step SCO around 166 K, [Fe(*2,6-naphthy*){Au(CN)$_2$]$_2$}·0,5PhNO$_2$].[48] Whereas the use of 1,6-naphthyridine (*1,6-naphthy*) as a ligand (structural isomer of *2,6-naphthy*) leads to a complex of the composition [Fe(*1,6-naphthy*)$_2$(Ag(CN)$_2$)$_2$], which exhibits hysteretic SCO behavior centered at room temperature.[49]

Moreover, functionalization of the pyrazine (*pz*) ligand and its derivatives can also lead to multi-step SCO materials.[50] Using 2-fluoropyrazine (*Fpz*) the SCO compound of composition [Fe(*Fpz*){Au(CN)$_2$]$_2$}] could be obtained, and it displays a hysteretic SCO characterized by small plateaus upon the HS → LS (at 91%) and LS → HS (at 23%) transformations.[51] Another interesting example is the complex [Fe(*Mepz*){Au(CN)$_2$}$_2$] (*Mepz* = 2-methylpyrazine) that undergoes an incomplete stepped SCO with T_{c1} = 170 K and T_{c2} = 308 K. Supposedly, this may be related to the existence of three Fe types due to *Mepz* ligand disorder. In contrast, the silver-containing analogue remains HS during the whole temperature range.[52]

The fact that the type and size of the substituent in the pyrazine ring have significant influences on SCO characteristics of iron(II) complexes based on it prompts the use of other 2-substituted pyrazines for the design of new switchable materials. Previous studies, as mentioned above,

included the use of halogens (F, Cl, I), alkyl (Me) and amino groups as substituents.[50–53] Therefore, to fully comprehend the effect of the substituent on SCO, as well as to expand the library of SCO complexes based on 2-substituted pyrazines, it was decided to use the aromatic substituent – phenyl. The presence of two aromatic rings in 2-phenylpyrazine theoretically implies the doubled number of π···π interactions. It was expected to afford enhanced cooperativity of SCO systems, as was observed for a similar example from the family of SCO complexes based on substituted pyridines.[54]

Here we report on the synthesis and comparative analysis of SCO properties of two 2D Hofmann-like frameworks with 2-phenylpyrazine (*Phpz*) of composition $[Fe(Phpz)_2\{M(CN)_2\}_2]$ (where M = Ag, Au).

■ EXPERIMENTAL SECTION

Materials and General Procedures. All chemicals were purchased from commercial suppliers and used without further purification. Anhydrous potassium dicyanoaurate ($K[Au(CN)_2]$) and anhydrous potassium dicyanoargentate ($K[Ag(CN)_2]$) were purchased from commercial sources (Sigma Aldrich). 2-Phenylpyrazine (*Phpz*) and methanol (MeOH) were provided by UkrOrgSyntez Ltd. Iron(II) *p*-toluenesulfonate hexahydrate ($Fe(OTs)_2{\cdot}6H_2O$) was obtained as previously described by Coucouvanis.[55]

Synthesis. Bulk polycrystalline forms of **AgPhpz** and **AuPhpz** were obtained by mixing alcohol solutions of $Fe(OTs)_2{\cdot}6H_2O$ (0.05 mmol in 0.25 mL of MeOH) and *Phpz* (0.20 mmol in 0.35 mL of MeOH), followed by the addition of an aqueous solution of $K[M(CN)_2]$ (M = Ag, Au) (0.10 mmol in 0.15 mL of H_2O). A yellow precipitate was removed by centrifugation, washed with MeOH and dried in air for 1 hour. Yields: 86.9% (**AgPhpz**), 47.8% (**AuPhpz**). Elemental Analysis of $C_{24}H_{16}Ag_2FeN_8$ (**AgPhpz**): calcd. C, 41.90; H, 2.34; N, 16.29; found C, 41.81; H, 2.40; N,

16.18%. FT-IR (cm^{-1}): 2153(m), 1523(w), 1469(m), 1447(m), 1401(m), 1302(w), 1188(w), 1149(s), 1125(s), 1085(m), 1046(w), 1025(m), 1012(w), 920(w), 852(m), 769(s), 739(w), 691(s), 662(w), 618(s), 568(s), 473(w), 428(s), 419(s), 406(s). Elemental Analysis of $C_{24}H_{16}Au_2FeN_8$ (**AuPhpz**): calcd. C, 33.28; H, 1.86; N, 12.94; found C, 33.43; H, 2.04; N, 12.91%. FT-IR (cm^{-1}): 2174(s), 1524(w), 1470(m), 1448(s), 1402(m), 1303(m), 1189(w), 1150(s), 1123(m), 1085(s), 1046(m), 1026(s), 1014(w), 919(w), 851(s), 768(s), 745(m), 695(s), 687(s), 662(m), 617(m), 568(s), 476(m), 426(s), 407(w). Elemental analyses (CHN) were performed with a Vario Micro Cube (Elementar) CHNOS elemental analyzer.

Single crystals of **AgPhpz** and **AuPhpz** were grown via a slow diffusion method within three layers in a 5 mL tube. 0.25 mL of an aqueous solution of $K[M(CN)_2]$ (M = Ag, Au) (0.05 mmol) was poured on the bottom of the tube. Then 2.5 mL of a water-methanol mixture (1:1) was gently layered on top. The third layer was a solution (0.5 mL) of $Fe(OTs)_2 \cdot 6H_2O$ (0.025 mmol) and *Phpz* (0.10 mmol) in MeOH. Yellow crystals were obtained in the second layer after 2 weeks. Crystals were kept under the mother solution prior to the subsequent measurements. It should be noted that it is important to adhere to the proportions and mixing sequence, since for **AuPhpz** there is a certain probability of the production of a coordination compound $[Fe(CN)_2(Phpz)_2(H_2O)_2][Au(CN)_2]$.[56]

X-ray Diffraction. Single-crystal X-ray diffraction data were collected on Oxford-Diffraction XCALIBUR Eos CCD diffractometer with graphite-monochromated Mo-Kα radiation at 293, 147, 110 K (for **AgPhpz**) and at 296, 200, 112 K (for **AuPhpz**). The unit cell determination and data integration were carried out using the CrysAlisPro package from Oxford Diffraction. Multi-scan correction for absorption was applied. The structures were solved with ShelXT program using intrinsic phasing method and refined by full-matrix least-squares method on F^2 with ShelXL.[57,58]

Olex2 was used as an interface to the ShelX programs.[59] Non-hydrogen atoms were refined anisotropically. Aromatic hydrogen atoms were geometrically fixed and refined using a riding model. Detailed crystallographic data for **AgPhpz** and **AuPhpz** are provided in the Supporting Information (SI, Crystallographic Tables). Specific details of each refinement are given in the crystallographic information files (CIF-files). The distortion parameters (Σ) were calculated using the OctaDist tool.[60]

Magnetic measurements. Temperature-dependent magnetic susceptibility measurements were carried out using a MPMS3 SQUID magnetometer (Quantum Design Inc., San Diego, CA, USA) in DC mode, under a DC magnetic field of 1000 Oe, with a heating/cooling rate of 2 K min^{-1}, in the temperature region 50–250 K for **AgPhpz** and 100–300 K for **AuPhpz**. These regions were selected based on the preliminary optical experiments. **AgPhpz** (13.49 mg) or **AuPhpz** (5.16 mg) (bulk polycrystalline form) was loaded into a gelatin cap, which was placed in a plastic straw and then inserted in SQUID chamber at room temperature. Sample's position was identified at room temperature. All data were corrected for the diamagnetic contributions of the cap and the compound (estimated from Pascal's constants).[61]

Mössbauer measurements. The Mossbauer spectra for **AgPhpz** sample were measured at 290, 147 and 90 K using a MC-1104E Mössbauer spectrometer equipped with a liquid nitrogen cryostat. A ^{57}Co source embedded in a Cr matrix and activity of about 10 mCi was used. Fitting of the experimental data was performed with OriginPro software. All isomer shift values are relative to sodium nitroprusside at room temperature with the next recalculation relative to α-Fe. Mössbauer spectra for **AuPhpz** sample were measured at 293, 200 and 90 K using a constant acceleration Mössbauer spectrometer equipped with a liquid nitrogen cryostat. A ^{57}Co source embedded in a

Rh matrix and activity of ~25 mCi was used. Fitting of the experimental data was performed with OriginPro software. All isomer shifts are given relatively to iron metal at room temperature.

Raman spectroscopy. Raman spectra were recorded using Horiba Scientific LabRam HR Evolution spectrometer in the 25–1650 cm^{-1} frequency range. Green laser with 1% ND filter was used for Raman excitation at 532 nm. Temperature control was realized using Linkam THMS 600 cryostat. The following parameters were used: acquisition time 100 s; 3 accumulations; grating 600 gr/mm.

FT-IR spectroscopy. IR spectra were recorded with a Spectrum Two spectrometer (PerkinElmer Inc., Waltham, MA, USA) in attenuated total reflectance (ATR) mode in ambient conditions. Spectra were recorded at 4 cm^{-1} resolutions. Wavelength range: 3500–400 cm^{-1}. Variable temperature IR measurements were performed in the 625−4000 cm^{-1} spectral range in transmittance mode on a Nicolet Nexus 470 spectrometer. Samples of **AgPhpz** and **AuPhpz** were homogenized in liquid paraffin and placed between two KBr pellets. IR spectra were collected with vacuumized Specac cryo-cell cooled with liquid nitrogen in the temperature range 100–290 K. Temperature control was realized using Specac Variable Temperature Cell Controller.

Optical measurements. The system for monitoring the SCO by changing the intensity of the reflected light for bulk polycrystalline forms of both complexes consisted of an optical microscope Optica SZM-1 equipped with the optical camera Sigeta UCMOS 1300. The system for monitoring the SCO by changing the intensity of the transmitted light for single crystals of both complexes consisted of an optical microscope MICROmed XS-8530 equipped with a ×10 long working-distance objective (numerical aperture, NA = 0.25) and a CCD MICROmed camera 5.0 mPix. The sample temperature was controlled with a Linkam optical cryostat DSC600. Cooling/heating rates were 0.5, 1, 5 and 10 K min^{-1}. Before starting experiment, we purged of the air from the stage

chamber with dry nitrogen. Photographs were taken automatically using ToupView software (for bulk polycrystalline forms) and Plugable Digital Viewer v3.1.07 software (for single crystals). Image processing was performed using ImageJ software.

■ RESULTS AND DISCUSSION

X-ray diffraction. To establish the crystal structure of the title compounds, single crystal X-ray diffraction analysis was carried out. The crystallographic data and structure refinements for complexes [Fe(*Phpz*)$_2${Ag(CN)$_2$}$_2$] (**AgPhpz**) and [Fe(*Phpz*)$_2${Au(CN)$_2$}$_2$] (**AuPhpz**) are summarized in Tables S4-S40 (see SI). Moreover, bulk polycrystalline forms of the complexes were examined using PXRD diffraction. This ancillary experiment confirmed the correspondence between of the structures of bulk polycrystalline forms and crystals for each complex. Thermal treatment (heating to 380 K) does not affect the structures as revealed by PXRD (Fig. S1-S3).

The crystal structure determination of **AgPhpz** was performed at 110 (LS), 293 (HS) and 147 K (plateau region corresponding to the HS/LS state). It was found that **AgPhpz** crystallizes in the monoclinic $P2_1/n$ space group, which is preserved at all temperatures. The structure contains a crystallographically unique Fe(II) center surrounded by two axial 2-phenylpyrazine ligands and four equatorial N-bound cyanide groups from two pairs of crystallographically independent $[Ag(CN)_2]^-$ bridges. The key structural fragment is shown in Figure 1a. The $[Ag(CN)_2]^-$ units bridge the Fe(II) ion parallel to the *bc* plane forming 2D $[Fe\{Ag(CN)_2\}_2]_\infty$ layers with (4,4)-net topology (Fig. 1b). $[Ag(CN)_2]^-$ bridges have an almost linear geometry of C–Ag–C moieties, e.g. the corresponding angles are 171.5(4)–172.5(4)° (at 293 K), 172.54(10)–172.91(10)° (at 147 K) and 171.9(4)–174.4(3)° (at 110 K).

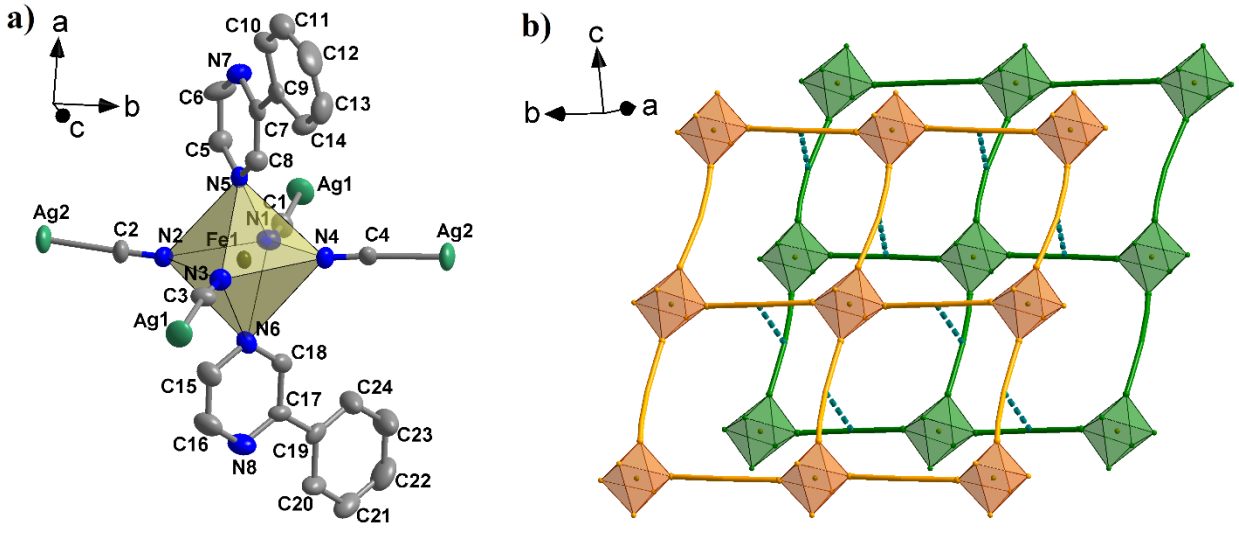

Figure 1. Crystal structure of **AgPhpz**: a) Representation of a key fragment of **AgPhpz**. Atom code: Fe (brown), Ag (green), N (blue), C (gray). Hydrogen atoms are omitted for clarity. b) View of the 2D $[Fe\{Ag(CN)_2\}_2]_\infty$ layers with (4,4)-net topology. Double-layered structure of **AgPhpz** supported by argentophilic Ag···Ag interactions (turquoise dash lines).

At 293 K, the average <Fe–N> bond length is 2.181(8) Å corresponding to the HS state of Fe(II) ions. At 147 K and 110 K, they are 2.071(2) and 1.970(8) Å, respectively, i.e., the average <Fe–N> bond lengths are shorter by 0.110 and 0.211 Å comparing to the HS form indicating the complete SCO achieved at 110 K. The average axial $Fe–N_{Phpz}$ bond lengths are larger than the equatorial $Fe–N_{CN}$ by 0.038 Å at 293 K and by 0.021 Å at 110 K. Moreover, the SCO provokes a gradual decrease of the polyhedral volume of FeN_6 from 13.801 $Å^3$ (293 K) to 10.177 $Å^3$ (110 K) with an intermediate value of 11.834 $Å^3$ at 147 K. The total change of the volume of the unit cell is 9.1%. At 293 K, the distortion parameter (Σ, the sum of deviations of the 12 "*cis*" N–Fe–N angles from 90°) is equal to 19.33°, while the Σ values of other two states are almost the same: 16.91° at 147 K and 16.88° at 110 K. Thus, as expected, the geometry around the coordination center in the HS

state is more distorted than in the HS/LS and LS states. Selected angles and bond lengths are given in Table 1.

Table 1. Selected angles and bond lengths for **AgPhpz** and **AuPhpz**.

	AgPhpz			**AuPhpz**		
T (K)	293	147	110	296	200	112
Spin state	HS	HS/LS	LS	HS	HS/LS	LS
<Fe–N>$_{average}$ (Å)	2.181(8)	2.071(2)	1.970(8)	2.165(12)	2.059(10)	1.967(14)
<Fe–N>$_{Phpz}$ (Å)	2.206(9)	2.090(2)	1.984(8)	2.226(12)	2.101(9)	1.998(14)
<Fe–N>$_{CN}$ (Å)	2.168(8)	2.062(2)	1.963(8)	2.135(11)	2.038(10)	1.952(12)
$V_{oct}(FeN_6)$ (Å^3)	13.801	11.834	10.177	13.508	11.625	10.140
∑ (°)	19.33	16.91	16.88	10.55	13.70	13.62
∠<C–M–C> (°)	172.0(4)	172.7(1)	173.2(4)	178.8(6)	179.5(5)	179.6(6)
∠<Fe–N≡C> (°)	172.8(8)	173.4(2)	174.4(7)	168.7(12)	171.4(10)	172.2(12)

As in other Hofmann-type SCO complexes with $[Ag(CN)_2]^-$ bridges, argentophilic Ag···Ag interactions are observed in **AgPhpz** (Fig. 1b). At 293 K, the length of Ag···Ag contacts is 3.0865(13) Å. Temperature decrease leads to the shortening of the Ag···Ag contacts, and they are 3.0617(3) Å (at 147 K) and 3.0361(10) Å (at 110 K). Moreover, the distance between two adjacent noninteracting layers (Fe1 to Ag2 distance) is reduced from 7.866(2) Å at 293 K to 7.7691(5) Å at 147 K and 7.704(2) Å at 110 K.

In addition, **AgPhpz** is characterized by a dense packing also due to various other supramolecular interactions. Selected parameters of supramolecular contacts are given in Table 2. The presence of more than one aromatic ring in the azine ligand leads to the fact that the packing of the 2-phenylpyrazine rings is held by different kinds of π···π stacking interactions (Fig. 2b).

There are two sets of short π-stacking with parallel-displaced (offset) conformation and two sets with T-shaped conformation (C–H···π interaction). As a result, such an advanced system of weak π-contacts leads to additional stabilization of the structure and the absence of a solvent accessible voids due to dense packing. 'Edge-to-face' contacts (C–H···π interaction) deserve more attention since are rarely found in Hofmann clathrates.[25,26] At 293 K, C13–H13···C''$_{ring}$ / C15–H15···C'$_{ring}$ distances are 2.964(4) / 3.142(5) Å (where C'$_{ring}$ is the centroid of C19C20C21C22C23C24 aromatic ring; C''$_{ring}$ is the centroid of N6C15C16N8C17C18 aromatic ring). They are 2.8718(10) / 3.0587(10) Å at 147 K and 2.791(4) / 2.9522(2) Å at 110 K. The offset π···π interactions are characterized by centroid-centroid distances of 3.589(6)–3.610(6) Å in the HS state, 3.5261(10)–3.5654(10) Å in the HS/LS state and 3.509(4)–3.545(4) Å in the LS state. These distances lie at the middle of the typical distance range for such supramolecular interactions (from 3.3 to 3.8 Å).[62,63] It should also be noted the presence of weak intermolecular C–H···Ag interactions (Fig. 2a). Since systems with this type of contacts (C–H···M, where M = metal) play an important role in catalysis due to their possible involvement in C–H bond activation.[64]

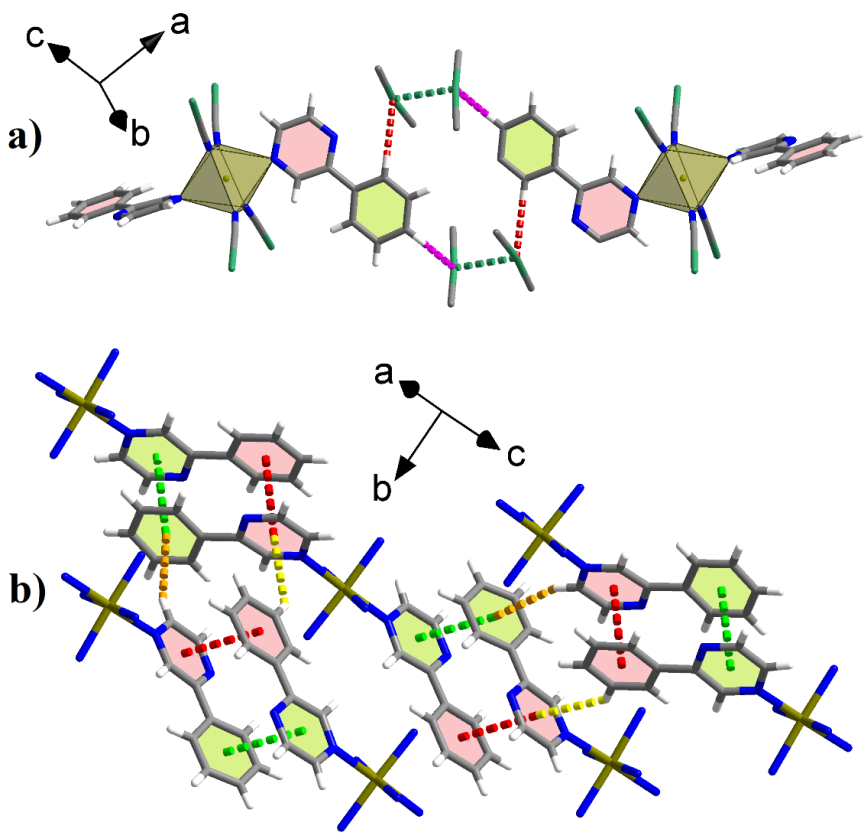

Figure 2. a) Supramolecular packing of **AgPhpz** via Ag···Ag (green dash lines) and C–H···M (pink and red dash lines) interactions. b) Supramolecular packing of **AgPhpz** via offset (green and red dash lines) and C–H···π (orange and yellow dash lines) π-contacts.

The compound **AuPhpz** crystallizes in the triclinic space group $P\bar{1}$ with two [Fe(*Phpz*)$_2${Au(CN)$_2$}$_2$] formula units per cell. **AuPhpz** contains only one crystallographically independent Fe(II) atom with the coordination environment of an elongated pseudo-octahedron [FeN$_6$] similar to **AgPhpz**. Each Fe(II) center binds four cyanide groups in *ab* plane and two axially coordinated crystallographic non-equivalent *Phpz* ligands. Two crystallographically distinct [Au(CN)$_2$]$^-$ bridges display virtually linear geometry. C–Au–C angles are 178.5(6)–179.0(5)°, 179.2(5)–179.7(4)° and 179.6(5)° at 296 K, 200 K and 112 K, respectively.

At 296 K, the average <Fe–N> bond length is 2.165(12) Å that corresponds to the HS state of Fe(II) site. At 200 K and 112 K they are 2.059(10) and 1.967(14) Å, respectively. The average <Fe–N> bond lengths are shorter by 0.106 Å (200 K) and 0.198 Å (112 K) comparing to HS form, clearly indicating a complete SCO achieved at 112 K. Like for **AgPhpz**, the average axial bond length Fe–N_{Phpz} in **AuPhpz** is always larger than the equatorial Fe–N_{CN}. The value of the polyhedral volume of FeN_6 drops from 13.508 $Å^3$ (296 K) to 10.140 $Å^3$ (112 K) with an intermediate value of 11.625 $Å^3$ at 200 K. The total change of the volume of the unit cell is 8.0%. It should be noted that the distortion parameter (Σ) value in **AuPhpz** increases with cooling: from 10.55° at 296 K (HS) to 13.70° at 200 K (HS/LS) and 13.62° at 112 K (LS). Thus, contrary to **AgPhpz**, the geometry around the coordination center in **AuPhpz** is the most distorted in the LS and HS/LS states. A similar behavior of Σ changes has already been reported for SCO analogues and other materials.[23,25,32,34,43,65]

An important structural feature of **AuPhpz** is the presence of strong aurophilic Au···Au interactions that support bilayer networks (Fig. 3a). At 296 K, the length of Au···Au contacts is 3.1072(8) Å. Temperature decrease leads to the shortening of the Au···Au contacts, and they are 3.0701(8) Å (at 200 K) and 3.0465(10) Å (at 112 K). Moreover, the distance between two adjacent noninteracting layers (Fe1 to Au2 distance) is reduced from 9.683(2) Å at 296 K to 9.584(2) Å at 147 K and 9.545(2) Å at 112 K. Also noteworthy is the lack of C–H···Au contacts in **AuPhpz**. Due to this, the **AuPhpz** structure is characterized by a larger than in **AgPhpz** distance between two adjacent noninteracting layers (Fe1 to M2) and the presence of small solvent accessible voids. The Olex2 software shows a total solvent accessible volume/cell of 7.6% (101.9 $Å^3$) at 296 K, 5.2% (65.9 $Å^3$) at 200 K and 4.3% (53.7 $Å^3$) at 112 K.

Table 2. Selected parameters of supramolecular contacts.

	AgPhpz			AuPhpz		
T (K)	293	147	110	296	200	112
Spin state	HS	HS/LS	LS	HS	HS/LS	LS
	Ag···Ag interaction			**Au···Au interaction**		
M···M (Å)	3.0865(13)	3.0617(3)	3.0361(10)	3.1072(8)	3.0701(8)	3.0465(10)
	offset π···π interactions					
C_{ring}–C'_{ring} (Å)	3.589(6)	3.5261(10)	3.509(4)	-	-	-
C''_{ring}–C'''_{ring} (Å)	3.610(6)	3.5654(10)	3.545(4)	-	-	-
C'_{ring}–C''_{ring} (Å)	-	-	-	3.666(11)	3.587(4)	3.499(2)
	C–H···π interactions					
C13–H13···C''_{ring} (Å)	2.964(4)	2.8718(10)	2.791(4)	-	-	-
∠C13–H13···C''_{ring} (°)	136.3(9)	135.7(2)	136.0(3)	-	-	-
C15–H15···C'_{ring} (Å)	3.142(5)	3.0587(10)	2.9522(2)	-	-	-
∠C15–H15···C'_{ring} (°)	153.6(7)	152.9(2)	150.8(5)	-	-	-
C16–H16···C'''_{ring} (Å)	-	-	-	2.650(4)	2.6014(2)	2.546(6)
∠C16–H16···C'''_{ring} (°)	-	-	-	142.7(12)	144.3(7)	146.4(2)
	C–H···M interactions					
C22–H22···Ag1 (Å)	2.6469(10)	2.6048(2)	2.5023(7)	-	-	-
C22···Ag1 (Å)	3.229(13)	3.142(2)	3.061(6)	-	-	-
∠C22–H22···Ag1 (°)	121.2(8)	117.27(13)	117.6(4)	-	-	-
C20–H20···Ag2 (Å)	2.6697(10)	2.6392(3)	2.5662(7)	-	-	-
C20···Ag2 (Å)	3.486(11)	3.460(2)	3.415(5)	-	-	-
∠C20–H20···Ag2 (°)	146.9(7)	147.49(15)	148.8(3)	-	-	-

where C_{ring} is the centroid of the aromatic ring (C_{ring}: N5C5H6N7C7C8;

C'_{ring}: C19C20C21C22C23C24; C''_{ring}: N6C15C16N8C17C18; C'''_{ring}: C9C10C11C12C13C14)

Like for **AgPhpz**, additional stabilization of **AuPhpz** structure is realized via short π···π stacking interactions (Fig. 3b). There are π-stacking with parallel-displaced (offset) and T-shaped (C–H···π interaction) conformations. It should be noted that the offset π···π contact is observed only in one of the two *Phpz* ligands (between aromatic rings N6C15C16N8C17C18 and C19C20C21C22C23C24) with the centroid···centroid distance of 3.666(11) Å in the HS state, 3.587(4) Å in the HS/LS state and 3.499(2) Å in the LS state. Another *Phpz* ligand forms only C–H···π interactions (Fig. 3b). Selected parameters of supramolecular contacts are given in Table 2.

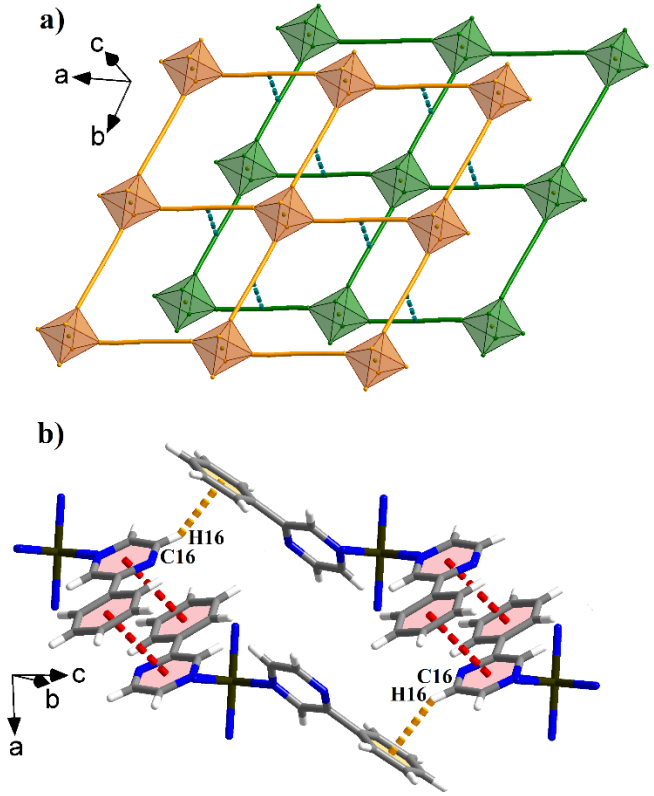

Figure 3. Crystal structure of **AuPhpz**: a) View of the 2D $[Fe\{Au(CN)_2\}_2]_\infty$ layers with (4,4)-net topology. Double-layered structure of **AuPhpz** supported by aurophilic Au···Au interactions (green dash lines). b) Supramolecular packing of **AuPhpz** via offset (red) and C–H···π (orange) π-contacts.

Comparing architectures of **AgPhpz** and **AuPhpz**, it is worth noting that both complexes at the plateau temperature have only one crystallographycally independent Fe(II) center, and the values of all structural parameters (including bond lengths and angles) have an "average" HS/LS character. Such behavior has already been observed for similar systems.[31,32] Moreover, due to the advanced system of supramolecular interactions both complexes do not contain guest molecules, although **AuPhpz** has small solvent accessible voids. Another distinctive feature of both complexes is the different behavior of structural changes in the coordination environment of the Fe(II) site upon SCO (the distortion parameter, Σ). The superposition of the HS and LS structures for both complexes show virtually ideal overlay of all structural fragments (Fig. S13-S18). Some minor displacements of atoms are mainly caused by a change in the Fe–N bond lengths by ~0.2 Å upon SCO. Comparison of the HS and LS structures with the HS/LS structure for **AgPhpz** shows some differences beyond the coordination sphere (contrary to **AuPhpz**) (Fig. S14-S15**)**. Thus, both distortion of cyanide $[Ag(CN)_2]^-$ bridges lying in the *bc* plane and a slight torsion of the 2-phenylpyrazine ligand are observed.

Magnetic measurements. The electronic reorganization in the Fe(II) ion during SCO causes a sharp change of magnetic susceptibility (χ_M). Thus, the temperature dependence of χ_M for bulk polycrystalline forms of complexes **AgPhpz** and **AuPhpz** were measured by superconducting quantum interference device (SQUID) in cooling and heating regimes (Fig. 4).

Complex **AgPhpz** undergoes a gradual two-step transition over the temperature range ~100 K (Fig. 4a) like for similar silver-containing SCO systems.[32,36,44] The $\chi_M T$ value is 3.53 cm^3 K mol^{-1} at 273 K, 1.86 cm^3 K mol^{-1} at 147 K, and 0.23 cm^3 K mol^{-1} at 50 K, which allows to roughly estimate the completeness of the transition 0%, 47%, and 94%, respectively. This corroborates with the complete stepped transformation of Fe(II) ion from the HS state (S = 2, paramagnetic) to

LS state (S = 0, diamagnetic). The transition temperatures are 175 (T_{c1}) and 125 K (T_{c2}) with a narrow pseudo-plateau appearing between 145 and 149 K. In the subsequent heating mode, these parameters are completely retained, and the transition curve reproduces the curve in cooling regime. It was found that **AgPhpz** is characterized by transition temperatures similar to silver-containing SCO complexes based on pyridine-type ligands.[33,36,44,66]

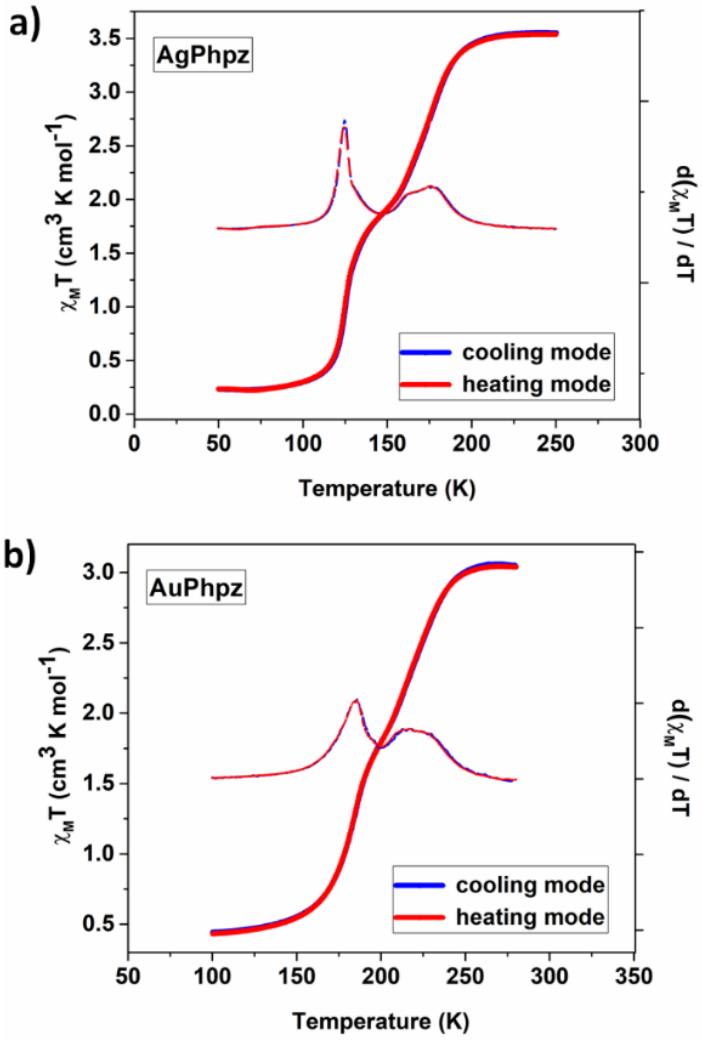

Figure 4. $\chi_M T$ vs. T plots for bulk polycrystalline forms of **AgPhpz** (a) and **AuPhpz** (b) in the selected transition area showing gradual temperature induced two-step SCO in these complexes. Derivative curves $d(\chi_M T)/dT$ are plotted.

The $\chi_M T$ value of **AuPhpz** is 3.06 cm^3 K mol^{-1} at 273 K, indicating the HS state of Fe(II) ion. Upon further cooling, $\chi_M T$ gradually decreases to 0.43 cm^3 K mol^{-1} at 100 K corresponding to the practically complete LS fraction. Two-step SCO behavior with critical temperatures of T_{c1} = 216 K and T_{c2} = 185 K is revealed by the differential $d(\chi_M T)/dT$ versus T plots (Fig. 4b). The $\chi_M T$ value at the midpoint of the pseudo-plateau is 1.80 cm^3 K mol^{-1} at 200 K, corresponding to a resultant 41% HS fraction. It should be noted that **AuPhpz** undergoes a more gradual two-step SCO (over ~110 K) with higher transition temperatures compared to **AgPhpz**. The difference in transition temperatures can be explained by different cooperative effects in these compounds caused by slightly different set of supramolecular interactions. A nice similar example is complexes based on 4-methylpyrimidine of composition $[Fe(4\text{-methylpyrimidine})_2[M^I(CN)_2]_2]$ (where M^I = Ag, Au), where the silver analogue has lower transition temperature comparing to the gold analogue. In that case the difference is also explained from the point of different crystal packing effects: presence of M···M interactions, M···N contacts and other structural features.[24,67]

Because of the spin-orbit interaction, the experimental value of $\chi_M T$ for the HS state of both complexes is higher than one calculated based on the spin of Fe(II) and equal to ~3.1–3.5 cm^3 K mol^{-1}. These $\chi_M T$ values are typical for most Fe(II) Hofmann-like clathrates reported previously (~3.0–3.8 cm^3 K mol^{-1}).[2,8,68] A small positive magnetization at low temperature (0.23 cm^3 K mol^{-1} (at 50 K) for **AgPhpz** and 0.43 cm^3 K mol^{-1} (at 100 K) for **AuPhpz**) is observed. Contribution of some HS Fe(II) impurities may be suspected, however their quantities are small enough that they are not seen on Mössbauer spectra (Fig. 5). A similar magnetic behavior was previously observed for different Hofmann-type coordination polymers.[2,8,69,70]

Gradual SCO at both steps in **AgPhpz** and **AuPhpz** indicates a weak cooperativity between metallic centers as compared to high-temperature hysteretic behavior of complexes based on unsubstituted pyrazine of the composition [Fe(*pz*){M(CN)$_2$}$_2$] (M = Ag, Au).[71,72] Thus, it can be concluded that the introduction of a bulky phenyl substituent to the pyrazine ring makes azine ligand being monodentate, that in its turn affects the SCO properties of both complexes (although, there is no any straightforward explanation of the nature of two-step transitions). The phenyl group sterically blocks the nearest donor nitrogen atom of the pyrazine ligand, which is a potential axial coordination donor. This makes 2-phenylpyrazine ligand similar to pyridine-type ligands, which frequently lead to the formation of multi-step SCO complexes with transition temperatures below RT. Also, it was already shown in previous studies that some SCO complexes based on 2-substituted pyrazines exhibit low-temperature two-step transitions.[50,51]

Because of the gradual character of SCO in both complexes, DSC is poorly suitable to monitor spin state change in these compounds. DSC peaks can be observed only at high scan rates (50-80 K min^{-1}), although the phase transition temperatures are reasonably well consistent with the temperatures found in magnetic measurements (Fig. S11-S12). Peaks for **AgPhpz** are resolved, while for **AuPhpz** only one peak is emerged.

Mössbauer measurements. SCO in **AgPhpz** and **AuPhpz** was investigated by the ^{57}Fe Mössbauer spectroscopy (Fig. 5) since this method provides direct information about the spin state and oxidation state of iron atom. The Mössbauer parameters for **AgPhpz** and **AuPhpz** in HS, HS/LS and LS states are summarized in Table 3.

Table 3. Hyperfine parameters for **AgPhpz** and **AuPhpz**.

	AgPhpz	**AuPhpz**

T (K)	290	147	90	293	200	90
Spin state	HS	HS/LS	LS	HS	HS/LS	LS
δ (mm s^{-1})	1.081(2)	1.19(4) (HS) 0.45(3) (LS)	0.489(2)	1.074(2)	1.142(5) (HS) 0.467(4) (LS)	0.528(2)
$\|\Delta E_Q\|$ (mm s^{-1})	1.095(3)	1.37(8) (HS) 0.10(5) (LS)	0.104(8)	0.801(4)	1.062(10) (HS) 0.084(32) (LS)	0.119(9)
Γ/2 (mm s^{-1})	0.121(3)	0.128(7) (HS) 0.109(7) (LS)	0.121(5)	0.158(3)	0.167(6) (HS) 0.164(11) (LS)	0.141(5)
Content (%)	100.0	48.8(21) (HS) 51.2(15) (LS)	100.0	100.0	52.5(16) (HS) 47.5(14) (LS)	100.0

At RT, the Mössbauer spectra of both **AgPhpz** and **AuPhpz** consist of one doublet, the hyperfine parameters (isomer shift (δ) and quadrupole splitting (ΔE_Q)) of which indicate that all the Fe(II) sites in both complexes are in the HS state (**AgPhpz**: δ = 1.081(2) mm s^{-1}, ΔE_Q = 1.095(3) mm s^{-1}; **AuPhpz**: δ = 1.074(2) mm s^{-1}, ΔE_Q = 0.801(4) mm s^{-1}). At temperatures corresponding to the HS/LS state, the Mössbauer spectra consist of two doublets in approximately 1:1 HS/LS ratio (48.8:51.2 for **AgPhpz** and 52.5:47.5 for **AuPhpz**), which corroborates with the magnetic measurements. A further decrease in temperature down to 90 K leads to an increase in the content of LS phase to 100%, which corresponds to the complete spin state change from HS to LS. δ and ΔE_Q values are typical for Fe(II) ion in the LS state (**AgPhpz**: δ = 0.489(2) mm s^{-1}, ΔE_Q = 0.104(8) mm s^{-1}; **AuPhpz**: δ = 0.528(2) mm s^{-1}, ΔE_Q = 0.119(9) mm s^{-1}). The values of half width at half maximum (Γ/2) lie in the range of 0.12-0.17 mm s^{-1}. Thus, the hyperfine parameters of both complexes are comparable with the corresponding values for related Hofmann-type complexes with dicyanometallic $[M(CN)_2]^-$ (M = Ag, Au) fragments.[33] The values of Γ/2 suggest these are individual Fe(II) compounds and there is a single Fe(II) site in each compound.

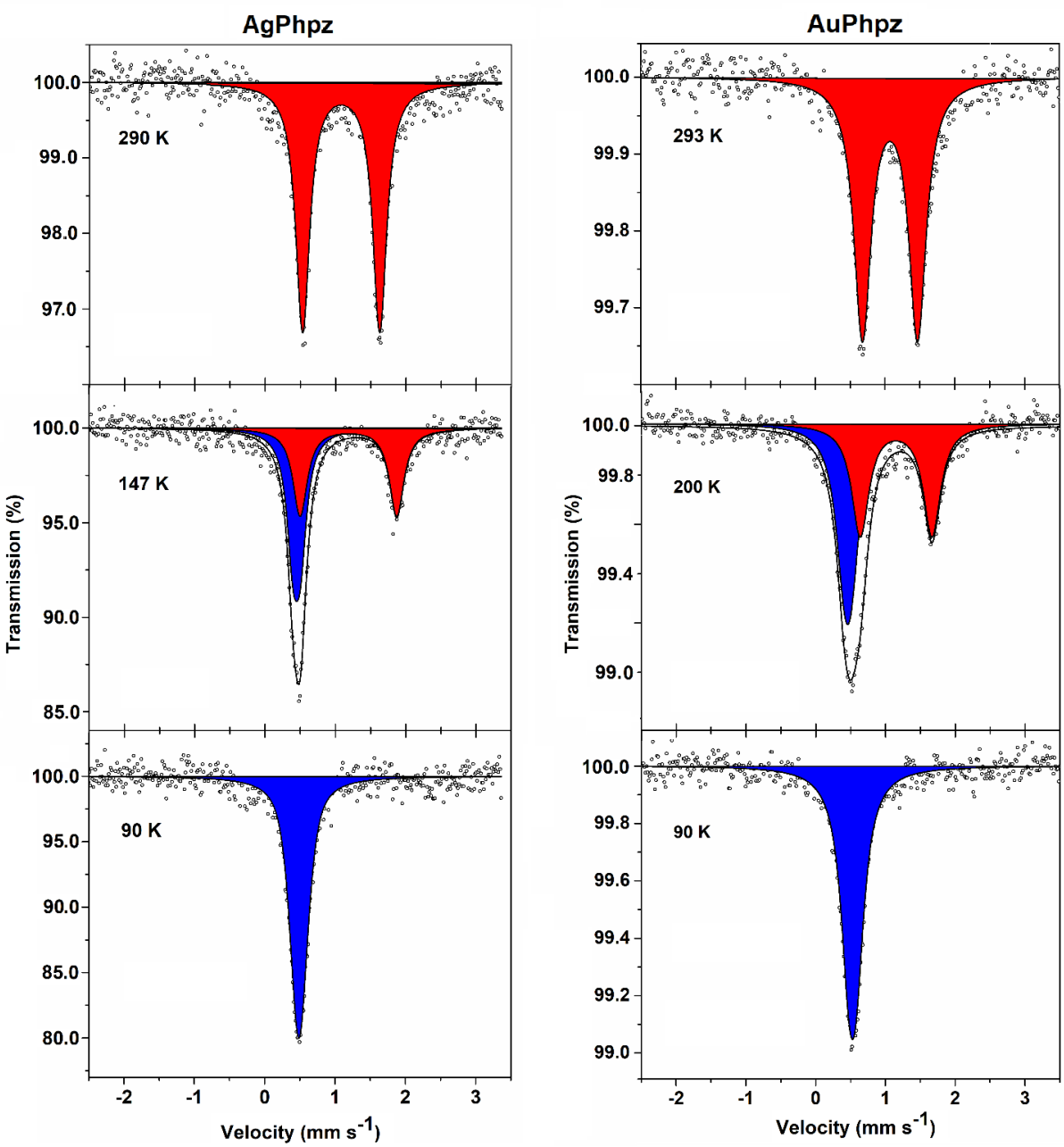

Figure 5. Mössbauer spectra of **AgPhpz** and **AuPhpz** recorded at HS, HS/LS and LS states. Both complexes display a complete SCO. Color codes: HS - red, LS - blue.

Spectroscopic measurements.

Raman spectroscopy is a powerful (complementary to magnetometry and ^{57}Fe Mössbauer spectroscopy) method to follow SCO.[73–80] E.g., complete disappearance of some characteristic

peaks and their appearance at different wavelengths confirm that SCO is complete in both directions (Fig. S9-S10). Figure 6 reveals the normalized intensity dependence on temperature for both complexes in the low-frequency spectral regions.

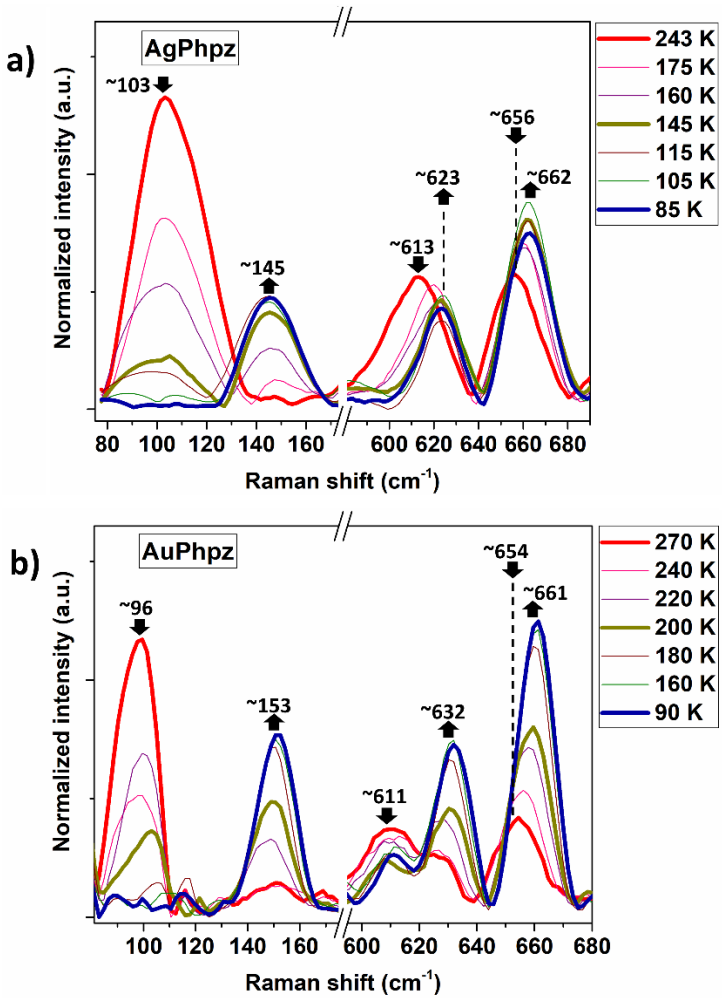

Figure 6. Raman spectra of **AgPhpz** (a) and **AuPhpz** (b) in the low-frequency spectral regions at various temperatures including temperatures corresponding to the HS, HS/LS and LS states.

It was found that the stretching mode attributed to Fe–N vibrations is shifted to the high-frequency region upon the spin state switches to the LS: from 103 to 145 cm^{-1} (Δ = 42 cm^{-1}) for **AgPhpz** and from 96 to 153 cm^{-1} (Δ = 57 cm^{-1}) for **AuPhpz**. In-plane bending vibrations of 2-phenylpyrazine are also affected by SCO. They exhibit shifts from 613 to 623 cm^{-1} (Δ = 10 cm^{-1})

/ from 656 to 662 cm^{-1} (Δ = 6 cm^{-1}) for **AgPhpz** and from 611 to 632 cm^{-1} (Δ = 21 cm^{-1}) / from 654 to 661 cm^{-1} (Δ = 7 cm^{-1}) for **AuPhpz**. Moreover, the increase of LS fraction causes a remarkable change in the intensity of the peaks at ~1150 and ~1300 cm^{-1}, which are also attributed to in-plane bending vibrations of *Phpz* (Fig. S9-S10).

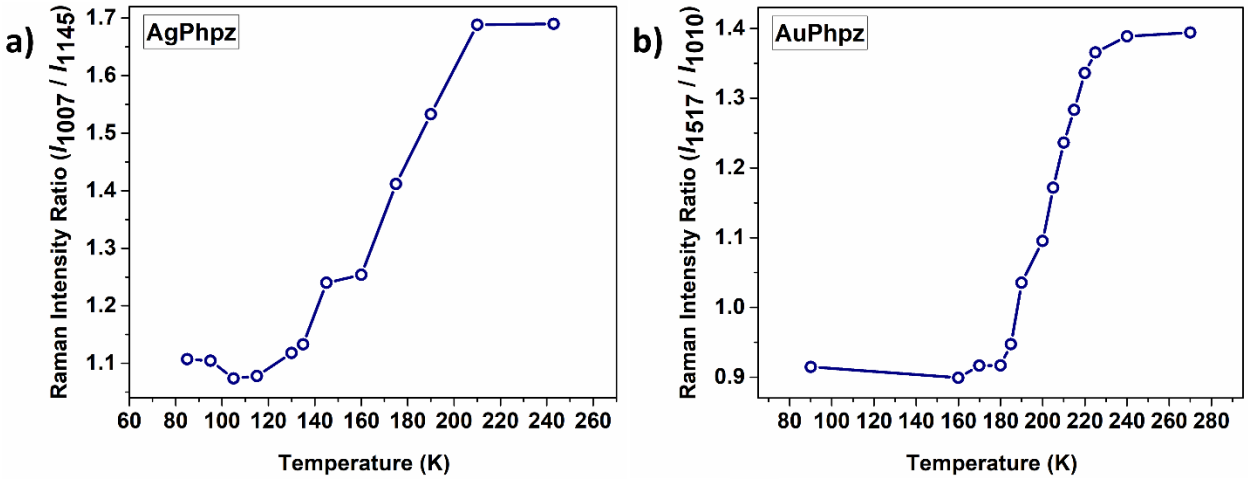

Figure 7. Temperature dependence of the intensity ratio of two Raman modes for bulk polycrystalline forms of **AgPhpz** (a) and **AuPhpz** (b).

The change of the spin state of iron(II) ions was also confirmed by plotting a curve from the intensity ratio of two Raman modes vs. temperature (Fig. 7). The plotted curves correspond to those obtained from magnetic and optical measurements. The equilibrium temperatures (**AgPhpz:** T_{c1} = 175 K and T_{c2} = 135 K; **AuPhpz**: T_{c1} = 205 K and T_{c2} = 185 K) are well consistent with the values obtained using other techniques.

In addition, variable temperature IR measurements for both complexes were performed. A few marker bands were used to follow SCO (Fig. S5-S8). Peaks at 637 cm^{-1} and 638 cm^{-1} are characteristic only for the LS state of **AgPhpz** and **AuPhpz**, respectively. The stretching peaks attributed to C≡N vibrations practically do not change their position upon SCO ($\Delta \approx 2$ cm^{-1}), but their intensity is affected.

Thus, all observed IR and Raman spectroscopy alterations clearly demonstrate the complete spin state change of Fe(II) and can be used as markers for monitoring SCO. The assignment of characteristic Raman and IR bands are summarized in Tables S1-S2. By comparing the vibrational modes in the HS and LS states of the obtained SCO systems with other known of Hofmann-like clathrates, it can be concluded that they follow the trend of the 2D structures with pyridine-like ligands.[73,74,80] This is evidenced by a minor shift of the C≡N vibrational band ($\leq$2 cm^{-1}) usually observed for 2D frameworks and the typical redshift.

Optical measurements. Two-step SCO behavior in single crystals and bulk polycrystalline forms of synthesized complexes has been monitored via optical microscopy since SCO is accompanied by color change. Bulks and single crystals of **AgPhpz** and **AuPhpz** are yellow at room temperature (HS), light orange in the HS/LS state and become bright orange upon cooling to 100 K (LS) (Fig. 8). Moreover, influence of the temperature scan rate on SCO behavior for different forms of these complexes has been studied. Temperature dependences of the normalized reflectance (for bulk polycrystalline forms) and normalized transmittance (for single crystals), recorded at various temperature scan rates, are given in Figure 8. The values of transition temperatures in both heating and cooling regimes are summarized in Table S3 (see SI).

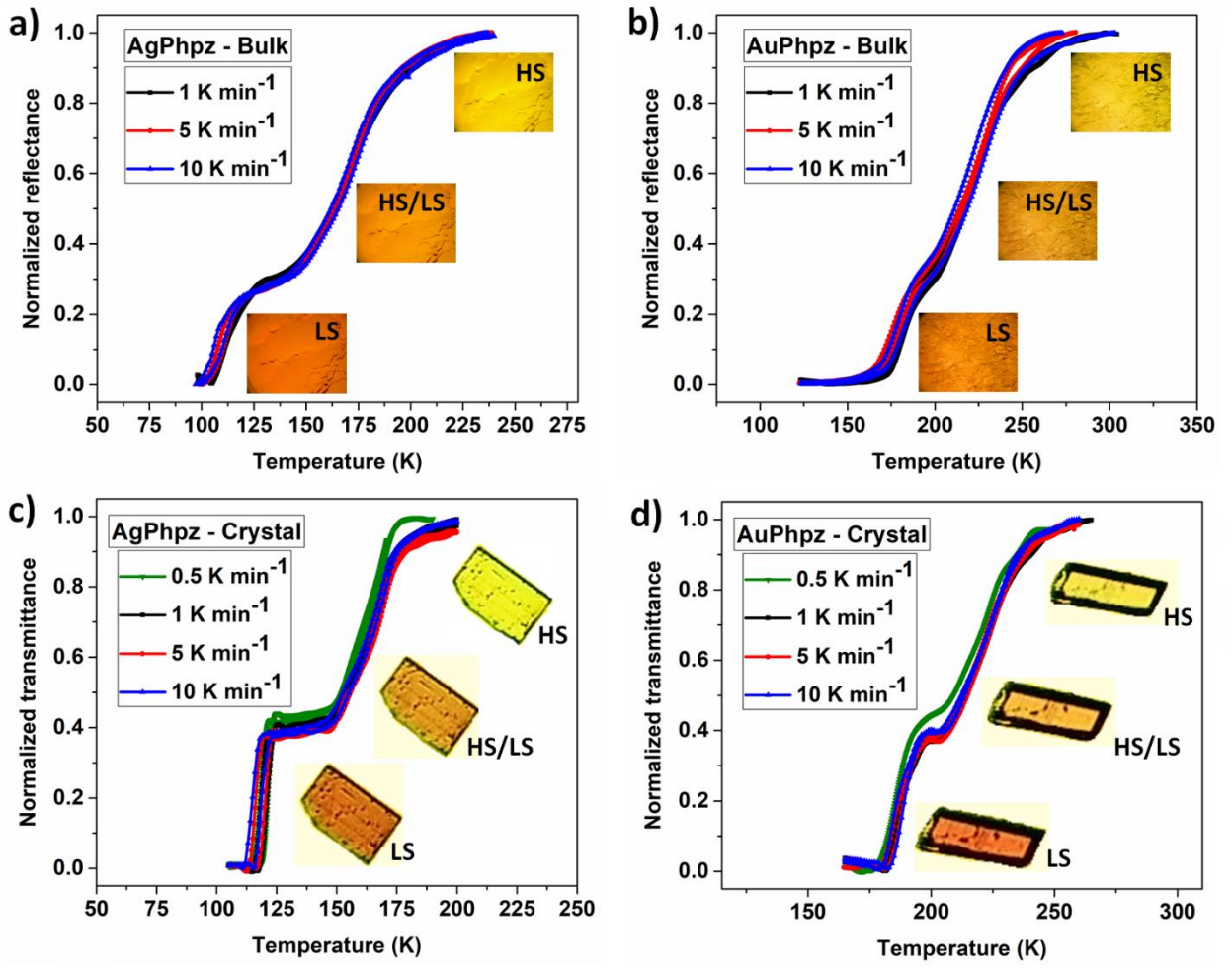

Figure 8. Temperature dependent optical studies of bulk polycrystalline forms of **AgPhpz** (a) and **AuPhpz** (b) (normalized optical reflectance vs. temperature) and single crystals of **AgPhpz** (c) and **AuPhpz** (d) (normalized optical transmittance vs. temperature) at different scan rates (0.5−10 K min^{-1}). The inserted pictures show the color evolution of **AgPhpz** and **AuPhpz** caused by SCO.

As expected, the minor difference in sharpness of SCO for bulk polycrystalline materials and the single crystals is observed. Because both forms usually show a different degree of cooperativity in the systems (the crystals show more cooperative SCO compared to powders).[49,81] This may lead to the appearance of kinetic effects. In our case, however, the kinetic effects are small compared to other examples in the literature; these minor changes can be as well cause by just thermalization

effects. It should also be noted that **AgPhpz** is characterized by a broader intermediate plateau (this is especially evident in case of single crystals: 21 K for **AgPhpz** vs. 5 K for **AuPhpz**), which is consistent with magnetic measurements data (Fig. 4) and can be explained by some structural differences between the complexes. **AgPhpz** is characterized by the presence of intermolecular C–H···Ag interactions and a more advanced system of weak π···π stacking interactions that potentially may stabilize the HS/LS state. Since optical microscopy is a semiquantitative method the HS/LS plateau does not correspond to the 50% change in the reflectance/transmittance for both **AgPhpz** and **AuPhpz** (in contrast to the magnetic curves). The reasons for this may be numerous factors: a slight increase in their opacity upon transition and just a small difference in color between HS and LS forms (yellow and orange, respectively). The collection and the treatment of images also contribute to the semiquantitative nature of the optical reflection/transmission methods used.

■ CONCLUSIONS

Two 2D Hofmann-like frameworks have been synthesized by self-assembly of Fe(II), *Phpz* and $[M(CN)_2]^-$ (M = Ag, Au) building blocks, and their SCO behavior has been thoroughly characterized. In contrast to the high-temperature hysteretic SCO complexes based on unsubstituted pyrazine (*pz*),[71,72] both synthesized complexes exhibit the gradual two-step SCO behavior at low temperatures. The nature of the two-step SCO remains enigmatic since the complexes at the plateau temperature have only one crystallographycally independent Fe(II) center, and the values of all structural parameters (including bond lengths and angles) have an "average" HS/LS character. Therefore, it is difficult to unambiguously indicate the reason of the two-step SCO behavior of these complexes; one can only assume that the presence of numerous

different supramolecular interactions such as metal-metal, C–H···M and π···π stacking contacts are responsible for this anti-cooperative behavior.

Thus, this research shows that slight modification of the axial ligand in cyanometallic frameworks can lead to a completely different SCO behavior. Moreover, the analysis shows the exceptional role of various supramolecular interactions in the structure and the influence of the bulky substituent in the ligand on the SCO behavior. As a result, the modification of the pyrazine ring can be used to fine-tuning the desired SCO properties for the design of new switchable materials.

■ ASSOCIATED CONTENT

Supporting Information. The Supporting Information (SI) contains experimental and calculated PXRD patterns, FT-IR and Raman spectra, DSC curves, images of superposition of structures **AgPhpz** and **AgPhpz**, crystal data and refinement details.

Accession Codes. CCDC 2116353-2116358 contain the supplementary crystallographic data for this paper. These data can be obtained free of charge via www.ccdc.cam.ac.uk/data_request/cif,or by emailing data_request@ccdc.cam.ac.uk, or by contacting The Cambridge Crystallographic Data Centre, 12 Union Road, Cambridge CB2 1EZ, UK; fax: +44 1223 336033.

■ AUTHOR INFORMATION

Corresponding Author

Il'ya A. Gural'skiy – Department of Chemistry, Taras Shevchenko National University of Kyiv, 01601 Kyiv, Ukraine; https://orcid.org/0000-0003-0944-6300;

Email: illia.guralskyi@univ.kiev.ua

Authors

Volodymyr M. Hiiuk – Department of Chemistry, Taras Shevchenko National University of Kyiv, 64 Volodymyrska St., 01601 Kyiv, Ukraine; Faculty of Natural Sciences, National University of Kyiv-Mohyla Academy, 2 Skovorody St., 04070 Kyiv, Ukraine; https://orcid.org/0000-0003-3665-6290

Sergii I. Shylin – Department of Chemistry – Ångström Laboratory, Uppsala University, 75120 Uppsala, Sweden; https://orcid.org/0000-0003-2104-1912

Diana D. Barakhtii – Department of Chemistry, Taras Shevchenko National University of Kyiv, 64 Volodymyrska St., 01601 Kyiv, Ukraine

Dmytro M. Korytko – Department of Chemistry, Taras Shevchenko National University of Kyiv, 64 Volodymyrska St., 01601 Kyiv, Ukraine

Volodymyr O. Kotsyubynsky – Department of Material Science and New Technology, Vasyl Stefanyk Precarpathian National University, 57 Shevchenko St., 76018 Ivano-Frankivsk, Ukraine

Aurelian Rotaru – Faculty of Electrical Engineering and Computer Science & Research Center MANSiD, Stefan cel Mare University, 13 Universitatii St., 720229 Suceava, Romania; https://orcid.org/0000-0002-8782-7988

Sergiu Shova – Ningbo University of Technology, No. 201, Fenghua Road, Ningbo City, Zhejiang, 315211, China; "Petru Poni" Institute of Macromolecular Chemistry, 41A Aleea Gr. Ghica Voda, 700487 Iasi, Romania; https://orcid.org/0000-0002-1222-4373

Author Contributions

The manuscript was written through contributions of all authors. All authors have given approval to the final version of the manuscript.

Notes

The authors declare no competing financial interest.

■ ACKNOWLEDGMENTS

This work has been supported by Ministry of Education and Science of Ukraine (grants 21BNN-06 and 19BF037-01M) and Horizon 2020 MSCA-RISE-2016 project 734322. Also, this work was supported by Romanian Ministry of Research, Innovation and Digitization, CNCS/CCCDI – UEFISCDI, project number PN-III-P1-1.1-TE-2019-2194 (Contract No. TE 123/2020) and project number PN-III-P4-ID-PCE-2020-2000 within PNCDI III (Contract No. 207/2021, PerMONSil). Volodymyr M. Hiiuk thanks Yuchymenko Family Endowment Fund for the financial support.

■ REFERENCES

(1) Gütlich, P.; Goodwin, H. A. (Eds.) Spin Crossover in Transition Metal Compounds I–III; Springer: Berlin/Heidelberg, Germany, **2004**.

(2) Muñoz, M. C.; Real, J. A. Thermo-, piezo-, photo- and chemo-switchable spin crossover iron(II)-metallocyanate based coordination polymers. *Coord. Chem. Rev.* **2011**, *255* (17–18), 2068–2093.

(3) Bousseksou, A.; Molnár, G.; Salmon, L.; Nicolazzi, W. Molecular spin crossover phenomenon: recent achievements and prospects. *Chem. Soc. Rev.* **2011**, *40* (6), 3313.

(4) Hauser, A. Spin-Crossover Materials. Properties and Applications. Edited by Malcolm A. Halcrow. *Angew. Chem. Int. Ed.* **2013**, *52* (40), 10419–10419.

(5) Gütlich, P.; Gaspar, A. B.; Garcia, Y. Spin state switching in iron coordination compounds. *Beilstein J. Org. Chem*. **2013**, 9, 342–391.

(6) Ohba, M.; Yoneda, K.; Agustí, G.; Muñoz, M. Carme.; Gaspar, A.; Real, J.; Yamasaki, M.; Ando, H.; Nakao, Y.; Sakaki, S.; Kitagawa, S. Bidirectional Chemo-Switching of Spin State in a Microporous Framework. *Angew. Chem. Int. Ed.* **2009**, *121* (26), 4861–4865.

(7) Kucheriv, O. I.; Oliynyk, V. V.; Zagorodnii, V. V.; Launets, V. L.; Gural'skiy, I. A. Spin-Crossover Materials towards Microwave Radiation Switches. *Sci. Rep.* **2016**, *6* (1), 38334.

(8) Kucheriv, O. I.; Fritsky, I. O.; Gural'skiy, I. A. Spin Crossover in Fe^{II} Cyanometallic Frameworks. *Inorganica Chim. Acta* **2021**, *521*, 120303.

(9) Manrique-Juárez, M. D.; Rat, S.; Salmon, L.; Molnár, G.; Quintero, C. M.; Nicu, L.; Shepherd, H. J.; Bousseksou, A. Switchable Molecule-Based Materials for Micro- and Nanoscale Actuating Applications: Achievements and Prospects. *Coord. Chem. Rev.* **2016**, *308*, 395–408.

(10) Ni, Z.-P.; Liu, J.-L.; Hoque, M. N.; Liu, W.; Li, J.-Y.; Chen, Y.-C.; Tong, M.-L. Recent advances in guest effects on spin-crossover behavior in Hofmann-type metal-organic frameworks. *Coord. Chem. Rev.* **2017**, *335*, 28–43.

(11) Ge, J.; Chen, Z.; Zhang, L.; Liang, X.; Su, J.; Kurmoo, M.; Zuo, J. A Two-Dimensional Iron(II) Coordination Polymer with Synergetic Spin-Crossover and Luminescent Properties. *Angew. Chem. Int. Ed.* **2019**, *58* (26), 8789–8793.

(12) Ghosh, S.; Kamilya, S.; Pramanik, T.; Rouzières, M.; Herchel, R.; Mehta, S.; Mondal, A. ON/OFF Photoswitching and Thermoinduced Spin Crossover with Cooperative Luminescence in a 2D Iron(II) Coordination Polymer. *Inorg. Chem.* **2020**, *59* (18), 13009–13013.

(13) Kucheriv, O. I.; Oliynyk, V. V.; Zagorodnii, V. V.; Launets, V. L.; Penkivska, O. V.; Fritsky, I. O.; Gural'skiy, I. A. Tunable microwave absorption of switchable complexes operating near room temperature. *RSC Adv.* **2020**, *10* (36), 21621–21628.

(14) Wang, M.; Li, Z.-Y.; Ishikawa, R.; Yamashita, M. Spin crossover and valence tautomerism conductors. *Coord. Chem. Rev.* **2021**, *435*, 213819.

(15) Kumar, K. S.; Ruben, M. Sublimable Spin-Crossover Complexes: From Spin-State Switching to Molecular Devices. *Angew. Chem. Int. Ed.* **2021**, *60* (14), 7502–7521.

(16) Kaushik, K.; Ghosh, S.; Kamilya, S.; Rouzières, M.; Mehta, S.; Mondal, A. Reversible Photo- and Thermo-Induced Spin-State Switching in a Heterometallic {*5d-3d*} W_2Fe_2 Molecular Square Complex. *Inorg. Chem.* **2021**, *60* (10), 7545–7552.

(17) Nihei, M.; Ui, M.; Yokota, M.; Han, L.; Maeda, A.; Kishida, H.; Okamoto, H.; Oshio, H. Two-Step Spin Conversion in a Cyanide-Bridged Ferrous Square. *Angew. Chem. Int. Ed.* **2005**, *44* (40), 6484–6487.

(18) Wei, R.-J.; Huo, Q.; Tao, J.; Huang, R.-B.; Zheng, L.-S. Spin-Crossover Fe^{II}_4 Squares: Two-Step Complete Spin Transition and Reversible Single-Crystal-to-Single-Crystal Transformation. *Angew. Chem. Int. Ed.* **2011**, *50* (38), 8940–8943.

(19) Klein, Y. M.; Sciortino, N. F.; Ragon, F.; Housecroft, C. E.; Kepert, C. J.; Neville, S. M. Spin crossover intermediate plateau stabilization in a flexible 2-D Hofmann-type coordination polymer. *Chem. Commun.* **2014**, *50* (29), 3838–3840.

(20) Piñeiro-López, L.; Seredyuk, M.; Muñoz, M. C.; Real, J. A. Two- and one-step cooperative spin transitions in Hofmann-like clathrates with enhanced loading capacity. *Chem. Commun.* **2014**, *50* (15), 1833–1835.

(21) Bao, X.; Guo, P. H.; Liu, W.; Tucek, J.; Zhang, W. X.; Leng, J. D.; Chen, X. M.; Gural'skiy, I.; Salmon, L.; Bousseksou, A.; Tong, M. L. Remarkably high-temperature spin transition exhibited by new 2D metal-organic frameworks. *Chem. Sci.* **2012**, *3* (5), 1629–1633.

(22) Zheng, C.; Jia, S.; Dong, Y.; Xu, J.; Sui, H.; Wang, F.; Li, D. Symmetry Breaking and Two-Step Spin-Crossover Behavior in Two Cyano-Bridged Mixed-Valence $\{Fe^{III}_2(\mu\text{-}CN)_4Fe^{II}_2\}$ Clusters. *Inorg. Chem.* **2019**, *58* (21), 14316–14324.

(23) Liu, W.; Peng, Y.; Wu, S.; Chen, Y.-C.; Hoque, M. N.; Ni, Z.; Chen, X.; Tong, M.-L. Guest-Switchable Multi-Step Spin Transitions in an Amine-Functionalized Metal-Organic Framework. *Angew. Chem., Int. Ed. Engl.* **2017**, *129* (47), 15178–15182.

(24) Kitase, K.; Kitazawa, T. A novel two-step Fe–Au type spin-crossover behavior in a Hofmann-type coordination complex $\{Fe(4\text{-methylpyrimidine})_2[Au(CN)_2]_2\}$. *Dalton Trans.* **2020**, *49* (35), 12210–12214.

(25) Zhang, C.-J.; Lian, K.-T.; Huang, G.-Z.; Bala, S.; Ni, Z.-P.; Tong, M.-L. Hysteretic four-step spin-crossover in a 3D Hofmann-type metal–organic framework with aromatic guest. *Chem. Commun.* **2019**, *55* (74), 11033–11036.

(26) Zhang, C.-J.; Lian, K.-T.; Wu, S.-G.; Liu, Y.; Huang, G.-Z.; Ni, Z.-P.; Tong, M.-L. The substituent guest effect on four-step spin-crossover behavior. *Inorg. Chem. Front.* **2020**, *7* (4), 911–917.

(27) Li, Z.-Y.; Dai, J.-W.; Shiota, Y.; Yoshizawa, K.; Kanegawa, S.; Sato, O. Multi-Step Spin Crossover Accompanied by Symmetry Breaking in an Fe^{III} Complex: Crystallographic Evidence and DFT Studies. *Chem. Eur. J.* **2013**, *19* (39), 12948–12952.

(28) Phonsri, W.; Davies, C. G.; Jameson, G. N. L.; Moubaraki, B.; Ward, J. S.; Kruger, P. E.; Chastanet, G.; Murray, K. S. Symmetry breaking above room temperature in an Fe(II) spin crossover complex with an N_4O_2 donor set. *Chem. Commun.* **2017**, *53* (8), 1374–1377.

(29) Ortega-Villar, N.; Muñoz, M.; Real, J. Symmetry Breaking in Iron(II) Spin-Crossover Molecular Crystals. *Magnetochemistry* **2016**, *2* (1), 16.

(30) Rodríguez-Velamazán, J. A.; Castro, M.; Palacios, E.; Burriel, R.; Kitazawa, T.; Kawasaki, T.; Rodrı, J. A. A Two-Step Spin Transition with a Disordered Intermediate State in a New Two-Dimensional Coordination Polymer. *J. Phys. Chem. B* **2007**, *111* (6), 1256–1261.

(31) Neville, S. M.; Leita, B. A.; Halder, G. J.; Kepert, C. J.; Moubaraki, B.; Létard, J.-F.; Murray, K. S. Understanding the two-step spin-transition phenomenon in Iron(II) 1D chain materials. *Chem. Eur. J.* **2008**, *14* (32), 10123–10133.

(32) Meng, Y.; Dong, Y.; Yan, Z.; Chen, Y.; Song, X.; Li, Q.; Zhang, C.; Ni, Z.; Tong, M. A New Porous Three-Dimensional Iron(II) Coordination Polymer with Solvent-Induced Reversible Spin-Crossover Behavior. *Cryst. Growth Des.* **2018**, *18* (9), 5214–5219.

(33) Rodríguez-Velamazán, J. A.; Carbonera, C.; Castro, M.; Palacios, E.; Kitazawa, T.; Létard, J.-F.; Burriel, R. Two-Step Thermal Spin Transition and LIESST Relaxation of the Polymeric Spin-Crossover Compounds $Fe(X\text{-}Py)_2[Ag(CN)_2]_2$ (X=H, 3-methyl, 4-methyl, 3,4-dimethyl, 3-Cl). *Chem. Eur. J.* **2010**, *16* (29), 8785–8796.

(34) Meng, Y.; Sheng, Q.-Q.; Hoque, M. N.; Chen, Y.; Wu, S.-G.; Tucek, J.; Zboril, R.; Liu, T.; Ni, Z.-P.; Tong, M.-L. Two-Step Spin-Crossover with Three Inequivalent Fe^{II} Sites in a Two-Dimensional Hofmann-Type Coordination Polymer. *Chem. Eur. J.* **2017**, *23* (42), 10034–10037.

(35) Liu, F.-L. L.; Tao, J. Hysteretic Two-Step Spin-Crossover Behavior in Two Two-Dimensional Hofmann-Type Coordination Polymers. *Chem. Eur. J.* **2017**, *23* (72), 18252–18257.

(36) Rodríguez-Velamazán, J. A.; Kitase, K.; Palacios, E.; Castro, M.; Fernández-Blanco, Á.; Burriel, R.; Kitazawa, T. Structural Insights into the Two-Step Spin-Crossover Compound Fe(3,4-dimethyl-pyridine)$_2[Ag(CN)_2]_2$. *Crystals* **2019**, *9* (6), 316.

(37) Kosone, T.; Tomori, I.; Kanadani, C.; Saito, T.; Mochida, T.; Kitazawa, T. Unprecedented three-step spin-crossover transition in new 2-dimensional coordination polymer$\{Fe^{II}$(4-methylpyridine)$_2[Au^{I}(CN)_2]_2\}$. *Dalton Trans.* **2010**, *39* (7), 1719–1721.

(38) Nihei, M.; Tahira, H.; Takahashi, N.; Otake, Y.; Yamamura, Y.; Saito, K.; Oshio, H. Multiple Bistability and Tristability with Dual Spin-State Conversions in $[Fe(dpp)_2][Ni(mnt)_2]_2 \cdot MeNO_2$. *J. Am. Chem. Soc.* **2010**, *132* (10), 3553–3560.

(39) Sciortino, N. F.; Scherl-Gruenwald, K. R.; Chastanet, G.; Halder, G. J.; Chapman, K. W.; Létard, J.-F.; Kepert, C. J. Hysteretic Three-Step Spin Crossover in a Thermo- and Photochromic

3D Pillared Hofmann-Type Metal-Organic Framework. *Angew. Chem. Int. Ed.* **2012**, *51* (40), 10154–10158.

(40) Clements, J. E.; Price, J. R.; Neville, S. M.; Kepert, C. J. Hysteretic Four-Step Spin Crossover within a Three-Dimensional Porous Hofmann-like Material. *Angew. Chem. Int. Ed.* **2016**, *55* (48), 15105–15109.

(41) Trzop, E.; Zhang, D.; Piñeiro-Lopez, L.; Valverde-Muñoz, F. J.; Carmen Muñoz, M.; Palatinus, L.; Guerin, L.; Cailleau, H.; Real, J. A.; Collet, E. First Step Towards a Devil's Staircase in Spin-Crossover Materials. *Angew. Chem. Int. Ed.* **2016**, *55* (30), 8675–8679.

(42) Zhang, D.; Trzop, E.; Valverde-Muñoz, F. J.; Piñeiro-López, L.; Muñoz, M. C.; Collet, E.; Real, J. A. Competing Phases Involving Spin-State and Ligand Structural Orderings in a Multistable Two-Dimensional Spin Crossover Coordination Polymer. *Cryst. Growth Des.* **2017**, *17* (5), 2736–2745.

(43) Sciortino, N. F.; Zenere, K. A.; Corrigan, M. E.; Halder, G. J.; Chastanet, G.; Létard, J.-F.; Kepert, C. J.; Neville, S. M. Four-step iron(II) spin state cascade driven by antagonistic solid state interactions. *Chem. Sci.* **2017**, *8* (1), 701–707.

(44) Valverde-Muñoz, F. J.; Bartual-Murgui, C.; Piñeiro-López, L.; Muñoz, M. C.; Real, J. A. Influence of Host–Guest and Host–Host Interactions on the Spin-Crossover 3D Hofmann-Type Clathrates $\{Fe^{II}(pina)[M^{I}(CN)_2]_2\}\cdot xMeOH$ (M^{I} = Ag, Au). *Inorg. Chem.* **2019**, *58* (15), 10038–10046.

(45) Piñeiro-López, L.; Valverde-Muñoz, F.-J.; Trzop, E.; Muñoz, M. C.; Seredyuk, M.; Castells-Gil, J.; da Silva, I.; Martí-Gastaldo, C.; Collet, E.; Real, J. A. Guest induced reversible

on–off switching of elastic frustration in a 3D spin crossover coordination polymer with room temperature hysteretic behaviour. *Chem. Sci.* **2021**, *12* (4), 1317–1326.

(46) Peng, Y.-Y.; Wu, S.-G.; Chen, Y.-C.; Liu, W.; Huang, G.-Z.; Ni, Z.-P.; Tong, M.-L. Asymmetric seven-/eight-step spin-crossover in a three-dimensional Hofmann-type metal–organic framework. *Inorg. Chem. Front.* **2020**, *7* (8), 1685–1690.

(47) Li, J.; Chen, Y.; Zhang, Z.; Liu, W.; Ni, Z.; Tong, M. Tuning the spin-crossover behaviour of a hydrogen-accepting porous coordination polymer by hydrogen-donating guests. *Chem. Eur. J.* **2015**, *21* (4), 1645–1651.

(48) Piñeiro-López, L.; Valverde-Muñoz, F. J.; Seredyuk, M.; Bartual-Murgui, C.; Carmen Muñoz, M.; Real, J. A.; Muñoz, M. C.; Real, J. A. Cyanido-Bridged Fe^{II}-M^{I} Dimetallic Hofmann-Like Spin-Crossover Coordination Polymers Based on 2,6-Naphthyridine. *Eur. J. Inorg. Chem.* **2018**, *2018* (3–4), 289–296.

(49) Hiiuk, V. M.; Shova, S.; Rotaru, A.; Ksenofontov, V.; Fritsky, I. O.; Gural'skiy, I. A. Room temperature hysteretic spin crossover in a new cyanoheterometallic framework. *Chem. Commun.* **2019**, *55* (23), 3359–3362.

(50) Kucheriv, O. I.; Shylin, S. I.; Ksenofontov, V.; Dechert, S.; Haukka, M.; Fritsky, I. O.; Gural'skiy, I. A. Spin Crossover in Fe(II)–M(II) Cyanoheterobimetallic Frameworks (M = Ni, Pd, Pt) with 2-Substituted Pyrazines. *Inorg. Chem.* **2016**, *55* (10), 4906–4914.

(51) Valverde-Muñoz, F. J.; Seredyuk, M.; Muñoz, M. C.; Znovjyak, K.; Fritsky, I. O.; Real, J. A. Strong Cooperative Spin Crossover in 2D and 3D Fe^{II}–$M^{I,II}$ Hofmann-Like Coordination Polymers Based on 2-Fluoropyrazine. *Inorg. Chem.* **2016**, *55* (20), 10654–10665.

(52) Shylin, S. I.; Kucheriv, O. I.; Shova, S.; Ksenofontov, V.; Tremel, W.; Gural'skiy, I. A. Hofmann-Like Frameworks Fe(2-methylpyrazine)$_n$[M(CN)$_2$]$_2$ (M = Au, Ag): Spin-Crossover Defined by the Precious Metal. *Inorg. Chem.* **2020**, *59* (9), 6541–6549.

(53) Gong, Y.; Li, Z. H.; Yan, X.; Wang, Y. Q.; Zhao, C. Y.; Han, W. K.; Hu, Q. T.; Lu, H. S.; Gu, Z. G. Bivariate Metal–Organic Frameworks with Tunable Spin-Crossover Properties. *Chem. Eur. J.* **2020**, *26* (54), 12472–12480.

(54) Seredyuk, M.; Gaspar, A. B.; Ksenofontov, V.; Verdaguer, M.; Villain, F.; Gütlich, P. Thermal- and Light-Induced Spin Crossover in Novel 2D Fe(II) Metalorganic Frameworks {Fe(4-PhPy)$_2$[M^{II}(CN)$_x$]$_y$}·sH$_2$O: Spectroscopic, Structural, and Magnetic Studies. *Inorg. Chem.* **2009**, *48* (13), 6130–6141.

(55) Coucouvanis, D. *Inorganic Syntheses*; Parry, R. W., Ed.; Inorganic Syntheses; John Wiley & Sons, Inc.: USA, **2002**; Vol. 33.

(56) Kucheriv, O. I.; Barakhtii, D. D.; Malinkin, S. O.; Shova, S.; Gural'skiy, I. A. Crystal structure of *catena*-poly[[gold(I)-μ-cyanido-[diaquabis(2-phenylpyrazine)iron(II)]-μ-cyanido] dicyanidogold(I)]. *Acta Crystallogr. Sect. E Crystallogr. Commun.* **2019**, *75* (8), 1149–1152.

(57) Sheldrick, G. M. Crystal structure refinement with SHELXL. *Acta Crystallogr. Sect. C Struct. Chem.* **2015**, *71* (1), 3–8.

(58) Sheldrick, G. M. A short history of SHELX. *Acta Crystallogr. Sect. A Found. Crystallogr.* **2008**, *64* (1), 112–122.

(59) Dolomanov, O. V.; Bourhis, L. J.; Gildea, R. J.; Howard, J. A. K.; Puschmann, H. OLEX2 : A complete structure solution, refinement and analysis program. *J. Appl. Crystallogr.* **2009**, *42* (2), 339–341.

(60) Ketkaew, R.; Tantirungrotechai, Y.; Harding, P.; Chastanet, G.; Guionneau, P.; Marchivie, M.; Harding, D. J. OctaDist: A tool for calculating distortion parameters in spin crossover and coordination complexes. *Dalton Trans.* **2021**, *50* (3), 1086–1096.

(61) Bain, G. A.; Berry, J. F. Diamagnetic Corrections and Pascal's Constants. *J. Chem. Educ.* **2008**, *85* (4), 532.

(62) Zhao, Y.; Li, J.; Gu, H.; Wei, D.; Xu, Y.; Fu, W.; Yu, Z. Conformational Preferences of π–π Stacking Between Ligand and Protein, Analysis Derived from Crystal Structure Data Geometric Preference of π–π Interaction. *Interdiscip. Sci. Comput. Life Sci.* **2015**, *7* (3), 211–220

(63) Janiak, C. A critical account on π–π Stacking in metal complexes with aromatic nitrogen-containing ligands. *J. Chem. Soc. Dalt. Trans.* **2000**, No. 21, 3885–3896.

(64) Brookhart, M.; Green, M. L. H.; Parkin, G. Agostic interactions in transition metal compounds. *Proc. Natl. Acad. Sci. U.S.A. P NATL ACAD SCI USA* **2007**, *104* (17), 6908–6914.

(65) Murphy, M. J.; Zenere, K. A.; Ragon, F.; Southon, P. D.; Kepert, C. J.; Neville, S. M. Guest Programmable Multistep Spin Crossover in a Porous 2-D Hofmann-Type Material. *J. Am. Chem. Soc.* **2017**, *139* (3), 1330–1335.

(66) Muñoz, M. C.; Gaspar, A. B.; Galet, A.; Real, J. A. Spin-Crossover Behavior in Cyanide-Bridged Iron(II)−Silver(I) Bimetallic 2D Hofmann-like Metal−Organic Frameworks. *Inorg. Chem.* **2007**, *46* (20), 8182–8192.

(67) Kitase, K.; Akahoshi, D.; Kitazawa, T. Effects of Both Methyl and Pyrimidine Groups in Fe–Ag Spin-Crossover Hofmann-Type Complex {Fe(4-Methylpyrimidine)$_2$[Ag(CN)$_2$]$_2$}. *Inorg. Chem.* **2021**, *60* (7), 4717–4722.

(68) Kosone, T.; Makido, Y.; Okuda, S.; Haigo, A.; Kawasaki, T.; Akahoshi, D.; Saito, T.; Kitazawa, T. Systematic Design of Crystal Structure for Hofmann-Like Spin Crossover Fe(L)$_2$[Ag(CN)$_2$]$_2$ Complexes. *Crystals* **2019**, *9* (7), 370.

(69) Liu, W.; Wang, L.; Su, Y.-J.; Chen, Y.-C.; Tucek, J.; Zboril, R.; Ni, Z.-P.; Tong, M.-L. Hysteretic Spin Crossover in Two-Dimensional (2D) Hofmann-Type Coordination Polymers. *Inorg. Chem.* **2015**, *54* (17), 8711–8716.

(70) Hiiuk, V. M.; Shova, S.; Rotaru, A.; Golub, A. A.; Fritsky, I. O.; Gural'skiy, I. A. Spin crossover in 2D Iron(II) phthalazine cyanometallic complexes. *Dalton Trans.* **2020**, *49* (16), 5302–5311.

(71) Gural'skiy, I. A.; Shylin, S. I.; Golub, B. O.; Ksenofontov, V.; Fritsky, I. O.; Tremel, W. High temperature spin crossover in [Fe(pyrazine){Ag(CN)$_2$}$_2$] and its solvate. *New J. Chem.* **2016**, *40* (11), 9012–9016.

(72) Gural'skiy, I. A.; Golub, B. O.; Shylin, S. I.; Ksenofontov, V.; Shepherd, H. J.; Raithby, P. R.; Tremel, W.; Fritsky, I. O. Cooperative High-Temperature Spin Crossover Accompanied by a Highly Anisotropic Structural Distortion. *Eur. J. Inorg. Chem.* **2016**, *2016* (19), 3191–3195.

(73) Molnár, G.; Niel, V.; Gaspar, A. B.; Real, J.-A.; Zwick, A.; Bousseksou, A.; McGarvey, J. J. Vibrational Spectroscopy of Cyanide-Bridged, Iron(II) Spin-Crossover Coordination Polymers:

Estimation of Vibrational Contributions to the Entropy Change Associated with the Spin Transition. *J. Phys. Chem. B* **2002**, *106* (38), 9701–9707.

(74) Hosoya, K.; Kitazawa, T.; Takahashi, M.; Takeda, M.; Meunier, J. F.; Molnár, G.; Bousseksou, A. Unexpected isotope effect on the spin transition of the coordination polymer $Fe(C_5H_5N)_2[Ni(CN)_4]$. *Phys. Chem. Chem. Phys.* **2003**, *5* (8), 1682–1688.

(75) Molnár, G.; Kitazawa, T.; Dubrovinsky, L.; McGarvey, J. J.; Bousseksou, A. Pressure tuning Raman spectroscopy of the spin crossover coordination polymer $Fe(C_5H_5N)_2[Ni(CN)_4]$. *J. Phys. Condens. Matter* **2004**, *16* (14), S1129–S1136.

(76) Ronayne, K. L.; Paulsen, H.; Höfer, A.; Dennis, A. C.; Wolny, J. A.; Chumakov, A. I.; Schünemann, V.; Winkler, H.; Spiering, H.; Bousseksou, A.; Gütlich, P.; Trautwein, A. X.; McGarvey, J. J. Vibrational spectrum of the spin crossover complex $[Fe(Phen)_2(NCS)_2]$ studied by IR and Raman spectroscopy, nuclear inelastic scattering and DFT calculations. *Phys. Chem. Chem. Phys.* **2006**, *8* (40), 4685–4693.

(77) Gnezdilov, V.; Lemmens, P.; Scheib, P.; Ghosh, M.; Pashkevich, Y. G.; Paulsen, H.; Schünemann, V.; Wolny, J. A.; Agustí, G.; Real, J. A. Spectrum-sensitive phonon wipeout due to a fluctuating spin state in a Fe^{2+} coordination polymer. *Phys. Rev. B* **2009**, *79* (4), 045122.

(78) Wolny, J. A.; Diller, R.; Schünemann, V. Vibrational Spectroscopy of Mono- and Polynuclear Spin-Crossover Systems. *Eur. J. Inorg. Chem.* **2012**, *2012* (16), 2635–2648.

(79) Lada, Z. G.; Andrikopoulos, K. S.; Chrissanthopoulos, A.; Perlepes, S. P.; Voyiatzis, G. A. A Known Iron(II) Complex in Different Nanosized Particles: Variable-Temperature Raman Study of Its Spin-Crossover Behavior. *Inorg. Chem.* **2019**, *58* (8), 5183–5195.

(80) Lada, Z. G.; Andrikopoulos, K. S.; Polyzou, C. D.; Tangoulis, V.; Voyiatzis, G. A. Monitoring the spin crossover phenomenon of [Fe(2-mpz)$_2$Ni(CN)$_4$] 2D Hofmann-type polymer nanoparticles via temperature-dependent Raman spectroscopy. *J. Raman Spectrosc.* **2020**, *51* (11), 2171–2181.

(81) Valverde-Muñoz, F. J.; Gaspar, A. B.; Shylin, S. I.; Ksenofontov, V.; Real, J. A. Synthesis of Nanocrystals and Particle Size Effects Studies on the Thermally Induced Spin Transition of the Model Spin Crossover Compound [Fe(phen)$_2$(NCS)$_2$]. *Inorg. Chem.* **2015**, *54* (16), 7906–7914.

Table of Contents (TOC) Graphic:

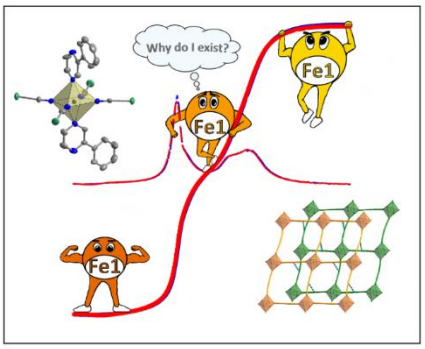

Manuscript synopsis:

Two 2D Hofmann-type coordination polymers of composition [Fe(*Phpz*)$_2${M(CN)$_2$}$_2$] (where *Phpz* = 2-phenylpyrazine; M = Ag, Au) have been synthesized and their spin-crossover (SCO) behavior has been thoroughly characterized by different techniques. Both complexes exhibit the highly reproducible two-step SCO behavior at low temperatures.